

# Recurrent Diffusion for Large-Scale Parameter Generation

Kai Wang

Dongwen Tang

Wangbo Zhao

Yang You

National University of Singapore

## Abstract

Parameter generation has struggled to scale up for a long time, significantly limiting its range of applications. In this study, we introduce *Recurrent diffusion for large-scale Parameter Generation*, called **RPG**. We first divide the trained parameters into non-overlapping parts, after which a recurrent model is proposed to learn their relationships. The recurrent model’s outputs, as conditions, are then fed into a diffusion model to generate the neural network parameters. Using only a single GPU, recurrent diffusion enables us to generate popular vision and language models such as ConvNeXt-L and LoRA parameters of LLaMA-7B. Meanwhile, across various architectures and tasks, the generated parameters consistently perform comparable results over trained networks. Notably, our approach also shows the potential to generate models for handling unseen tasks, which largely increases the practicality of parameter generation. Our code is available [here](#).

## 1. Introduction

Looking back on the journey of deep learning, the scaling up of neural networks is one of the most important keys to its remarkable success across various tasks [22, 33, 44]. In contrast, neural network parameter generation, from HyperNetworks [21] to recent diffusion-based methods [51, 66, 69], has struggled to scale up effectively, limiting its practical applications. As shown in Fig. 1, the scale gap between vision (or language) models and the generated parameters is at least  $10^4$ , posing significant challenges for this field.

To figure out the key challenges in scaling up parameter generation, we first analyze its unique requirements. Unlike traditional deep learning models that typically process data such as images or text, parameter generation involves network parameters in the training process. The size of parameters could be significantly larger than images or texts size. This fundamental difference in input format presents a significant challenge when scaling up. As the size of gen-

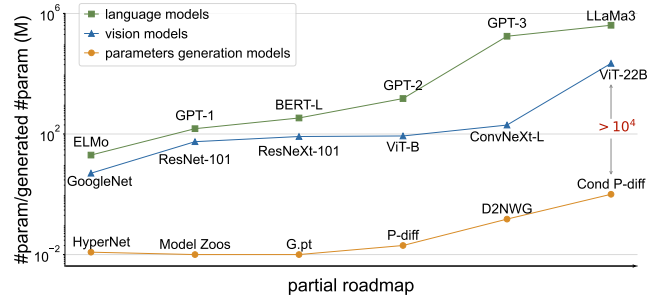


Figure 1. Partial roadmap of vision, language, and parameter generation models. Parameter number in vision or language models is at least  $10^4$  times larger than that of generated parameters.

erated parameters increases, the GPU memory requirement quickly becomes prohibitive.

Recently, p-diff [69] and D2N WG [66] attempted to address the challenge of balancing memory constraints with large-scale parameter generation. P-diff mainly generates a subset of the entire neural network parameters, while D2N WG employs a two-step process of synthesizing parameter parts and then combining them to form a complete model. However, these methods may overlook the inherent correlations among the parameter parts. To study the impact of these correlations, we conduct an experiment: exchanging partial parameters between two ViT-Tiny [14] models trained on CIFAR-10 [32] dataset. As illustrated in the following table, the significant performance degradation highlights the critical importance of parameter correlations.

model	ViT-Tiny A	partial A + partial B	ViT-Tiny B
acc. (%)	90.4	45.8	89.6

How can we model parameter relationships and leverage them for efficient parameter generation? Vision transformers often outperform CNNs by modeling patch relationships and capturing global information via self-attention. In language tasks, LLMs use next token prediction to model token relationships, capturing long-range dependencies. Inspired by these approaches, we can consider *treating parameter parts as tokens* in neural network parameter generation, potentially enabling methods to model inter-parameter relationships and capture dependencies.

\*Kai and Dongwen contributed equally.

In this paper, we propose **Recurrent diffusion for large-scale neural network Parameters Generation (RPG)**. Our approach first divides the trained network parameters into a set of non-overlapping parameter parts (simply called ‘tokens’ in the following). Subsequently, we use a recurrent model to learn the relationships among the tokens. Finally, the outputs of the recurrent model, as conditions, are fed into a diffusion process to generate the network parameters.

Our approach has the following properties: i) With a single GPU, our approach successfully synthesizes *full parameters* of large-scale vision models such as ResNet [22], ViT [14], and ConvNeXt [41] series, as well as LoRA [27] parameters of LLaMA-7B [67]. ii) Across various architectures and tasks, the generated parameters achieve comparable performance to the original models while exhibiting high diversity. iii) Empirical evidence suggests our approach has potential for generating models in unseen tasks. We anticipate that this work will inspire future research in large-scale parameter generation.

## 2. Related Works

**Diffusion models.** Diffusion models [13, 23, 48] gain increasing popularity in recent years, due to their superiority in image generation. Ever since its advent, many works have been done focusing on improving the generation quality and efficiency of diffusion models. For generation quality, Rombach et al. [55] propose to conduct diffusion in the latent space, enabling high-resolution image synthesis. Peebles and Xie [50] leverage the transformer [68] to explore scalability of diffusion models, proving the possibility of generating higher quality images by increasing model size. As for efficiency problem, efficient samplers [42, 64, 65], efficiency models [16, 62, 74], and global acceleration approaches [43, 49] are proposed to increase diffusion models’ efficiency. These methods facilitate generating high quality images with less computational and/or memory cost. Although diffusion models for image generation have achieved great success, how to improve quality and efficiency in large-scale parameter generation remains to be explored.

**Recurrent models.** Recurrent neural networks (RNNs) were first proposed to process sequential data, *i.e.*, the text. To tackle the vanishing gradient problem in early RNNs, long short-term memory (LSTM) [24, 25]. In recent years, transformer-based models [68] exhibits excellent potential in sequential data processing, due to their parallelized training and scalability. Although most transformers [53, 67] are used in auto-regressive manner, they can be seamlessly adapted to the recurrent paradigm. However, transformer-based models are suffering from the the quadratic complexity during their generation process, which greatly hinders their efficiency. Recently, various attempts, such as linear

attentions [7, 70], RWKV [52], Mamba [11, 19], and xL-STM [2], have been proposed to tackle this problem.

**Parameter generation.** The core idea of parameter generation is to learn the distribution of trained parameters. Stochastic neural networks [5, 18, 46, 57, 63, 71] and Bayesian neural networks [4, 17, 30, 31, 47, 54] model the priors or probability distributions over the parameters. These approaches mainly employ the learned prior knowledge of parameters to improve robustness and generalization, and to mitigate overfitting and uncertainties. However, these methods are limited by their generality to large-scale generation or more complex real-world scenarios.

HyperNetworks [21], *i.e.*, a small network, is proposed to generate various architectures’ parameters for a larger network. Smash [6] extends the range of architectures via a memory read-writes scheme. With the development of diffusion models, many works [8, 15, 29, 37, 38, 51, 66, 69] adopt diffusion models to generate neural network parameters. G.pt [51] collects 23 million checkpoints as the training data and uses conditional diffusion to learn the distribution of the parameters. Besides the heavy cost of collecting model parameters, G.pt can only generate less than 10K parameters. P-diff proposes unconditional diffusion to simulate the parameter updating. HyperRepresentations [58, 59, 61] use an autoencoder to capture the latent distribution of trained models. COND P-DIFF [29] and Tina [37] introduce task-controlled or text-controlled parameter generation method. Unfortunately, the above methods have a common drawback: *can not generate large-scale parameters, such as whole parameters of ResNet, ViT, ConvNeXt, or LoRA*. Therefore, our approach brings new inspiration to the field of parameter generation.

## 3. Large-Scale Parameter Generation

### 3.1. Overview

Our approach comprises two key components: parameter tokenization and recurrent diffusion. We show the inference process of recurrent diffusion in Fig. 2. The permutation state and position embedding are fed into the recurrent model. Then, the outputs of the recurrent model serve as conditions for the diffusion process, which generates the entire neural network parameters.

### 3.2. Parameter Tokenization

Inspired by the success of language and vision models [14, 68], we propose parameter tokenization that divides network parameters into non-overlapping tokens. Considering the distribution shifts across different layers, we first categorize the trained parameters according to their respective layer indices. Then, we apply normalization (subtracting the mean and dividing by the standard deviation) on each layer. These operations can be formulated as follows,

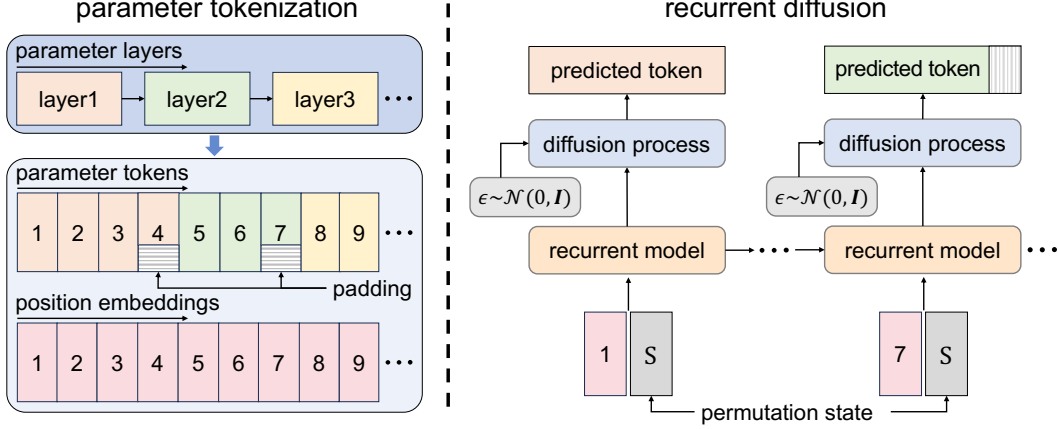


Figure 2. Illustration of the inference of the recurrent diffusion. The recurrent model takes permutation state and position embedding as inputs. The outputs of the recurrent model are then fed into the diffusion process as condition to synthesize the neural network parameters.

$$\begin{aligned}
 W &\xrightarrow{\text{divide by layer}} [w[1], \dots, w[i], \dots, w[I]] \\
 &\xrightarrow[-\mu \text{ and } /\sigma]{\text{normalize}} [\hat{w}[1], \dots, \hat{w}[i], \dots, \hat{w}[I]],
 \end{aligned} \quad (1)$$

where  $W$  denotes the trained parameters.  $\mu$  and  $\sigma$  denote the mean and standard deviation values of parameters.  $w_i$  and  $\hat{w}_i$  are the original and normalized parameters of the  $i$ -th layer, respectively.

The number of parameters varies across these layers, which is not conducive to efficient batch training. To this end, we slice each layer parameter into a set of tokens with the same token size, which can be written as follows,

$$\hat{w}[i] \xrightarrow{\text{tokenize}} K[i] = [k_i^1, \dots, k_i^j, \dots, \text{padding}(k_i^J)], \quad (2)$$

where the  $k_i^j$  represents the  $j$ -th token of  $i$ -th layer. For the last token of each layer, we apply padding operation to ensure that all layers have tokens of uniform length. It is worth noting that the padded regions are excluded from the loss calculation.

### 3.3. Recurrent Diffusion

**Permutation state.** Neural network symmetries [1, 34] do not affect the model outcomes but increase the difficulty of learning the parameter distribution. To address this, we introduce a unique state for each trained model  $W$  via one-hot embedding. This operation provides a guide for the generated parameters to mitigate the influence of parameter symmetries. For simplicity, we use  $S$  to represent the permutation state of  $W$ .

**Position embedding.** Inspired by ViT [14], we also encode the layer and token information described in the parameter tokenization (Sec. 3.2) using a two-dimensional sinusoidal position encoding. Specifically, the first dimension encodes

the layer index of the token in the original model, while the second dimension encodes the position of the token within its layer. For  $i$ -th layer parameter tokens  $K[i]$ , the position embedding can be formulated as follows,

$$K[i] \xrightarrow{\text{position embedding}} e[i] = [e_i^1, \dots, e_i^j, \dots, e_i^J], \quad (3)$$

where  $e_i^j$  denotes the position embedding of the parameters belong to  $j$ -th token of  $i$ -th layer.

**Recurrent model.** After obtaining the parameter tokens, permutation states, and position embeddings, we use a recurrent model to learn the representation of the parameter tokens. For clarity, we will refer to the output of the recurrent model as the ‘prototype’ in the following. This operation can be written as follows:

$$P_i^j, H_i^j = f(H_i^{j-1}, e_i^j, S), i \in [1, I], j \in [1, J], \quad (4)$$

where  $P_i^j$  and  $H_i^j$  denote the prototype and hidden state of the parameters belonging to  $j$ -th token of  $i$ -th layer, respectively.  $f(\cdot, \cdot, \cdot)$  denotes the state transition function. The structure of the recurrent model is simple. Considering efficiency, we use Mamba [20] followed by an MLP to project the feature dimension to the required size for the diffusion model. We also conduct ablation studies with other recurrent model architectures, such as LSTM [26] and transformer with its decoder in a causal manner [68].

**Parameter diffusion.** Inspired by p-diff [69] and MAR [35], we use 1D convolution to build the diffusion model. In this part, the parameter prototypes, serving as conditions, are fed into the diffusion process along with random noise. We optimize our approach through the following equation:

$$L_{\text{diff}} = \mathbb{E}_{t, K, \epsilon} [||\epsilon - \epsilon_{\theta}(K_t, t, P)||^2], \quad (5)$$

arch.\acc.(%)	params (M)	original	best	average	min
ResNet-18	11.7	70.0	69.9	69.5	69.0
ResNet-50	25.6	79.8	79.6	79.5	79.4
ViT-Tiny	5.7	74.9	75.4	75.3	75.2
ViT-Small	22.1	81.4	80.6	80.5	80.1
ViT-Base	86.6	84.4	84.6	84.4	84.2
ConvNeXt-Atto	3.7	75.2	74.6	74.4	74.2
ConvNeXt-Large	197.8	85.8	85.8	85.5	85.2

Table 1. We compare with the results of original models across seven architectures on the ImageNet-1K. Our approach successfully generates the entire model parameters that perform comparable results with the original models.

where  $K$ ,  $P$ ,  $L_{\text{diff}}$ , and  $t$  denote parameter tokens, prototypes, diffusion loss, and time step, respectively.  $\epsilon$  is Gaussian noise and  $\epsilon_{\theta}$  is the denoising network parameterized by  $\theta$ . Note that, the gradient propagates through  $P$  to the recurrent model, implicitly optimizing it as well.

## 4. Experiments

### 4.1. Setup

**Datasets and architectures.** We mainly evaluate our method across a wide range of tasks, including ImageNet-1K [12] for the classification, ADE20K [77] for the semantic segmentation, COCO [39] for the object detection, and BoolQ [9], PIQA [3], SIQA [56], HellaSwag [75], and ARC [10] for the commonsense reasoning tasks. To verify the scalability of our approach, we conduct experiments on various architectures with parameter counts ranging from several to hundred million. Details of parameter counts can be found in Tab. 1, 2, 3.

**Trained parameters collection.** We take parameters collection on the ImageNet-1K as an example. To save the cost, we finetune the full parameters of the models released in timm<sup>1</sup> and save 50 checkpoints as the training data. For each checkpoint, we assign a unique permutation state to guide the generated parameters.

**Training details.** We default to using Mamba [20] as the architecture of the recurrent model. The length of parameter tokens, permutation states, position embeddings, and prototypes is set to 8192. It is worth noting that the permutation states and position embeddings are fixed during the training by default. We also study the influence of the token length, varying it from 1024 to 16384. The parameter diffusion consists of 1D convolutional layers. More details about the model architectures, hyperparameters, and training process can be found in Appendix B.1.

**Inference details.** We input permutation states and position embeddings into the recurrent model to generate the prototypes. Then, the diffusion model utilizes the prototypes as

conditions, along with random noises, to synthesize the entire network parameters. We repeat the above process 10 times and report the best, average, and minimum.

### 4.2. Results of Large-Scale Parameter Generation

In this section, we present the results of our approach across a range of tasks including classification, semantic segmentation, object detection&instance segmentation, and language tasks. As most previous works encounter the out-of-memory issue at million-scale parameter generation, we mainly compare with the results from the trained networks, which we denote as ‘original’.

**Results on ImageNet-1K.** Tab. 1 presents performance comparisons across seven architectures on ImageNet-1K [12]. These architectures encompass the ResNet [22], ViT [14], and ConvNeXt [41] series, with parameter counts ranging from 3 to 197 million. Based on the results in Tab. 1, several crucial observations can be made as follows: i) Our approach successfully generates model parameters at hundred-million scales, overcoming the out-of-memory issues faced by previous works [29, 51, 66, 69]. ii) The performances of the generated models are comparable with the original ones.

method	ADE20K		COCO	
	mIoU(%)	mAcc(%)	mAP Bbox (%)	mAP Seg (%)
original	47.6	58.3	43.6	39.0
ours	47.1	57.5	44.5	39.6

Table 2. Accuracy comparison of original and generated parameters on ADE20K (176.5M parameters) and COCO (110.9M parameters). All models are built based on ViT-Base [14].

**Results on ADE20K and COCO.** We also investigate the generalization of our approach to semantic segmentation as well as object detection and instance segmentation tasks. We choose ADE20K [77] and COCO [39] as our benchmark datasets. For semantic segmentation, following Zhao et al. [76], we adopt UperNet [72] as the segmentation model and train it on ADE20K to prepare checkpoints. For object detection and instance segmentation, we finetune ViTDet [36] on COCO to collect checkpoints and report the results of mAP Bbox and mAP Seg, respectively. All experiments here are conducted based on ViT-B [14]. Tab. 2 presents the strong generalization of our approach to these two tasks. Specifically, compared to the original models, we achieve comparable or even slightly better results over all the above metrics.

**Results on commonsense reasoning.** We conduct experiments on language tasks to evaluate the generalization of our approach. We employ DoRA [40], an upgraded version of LoRA [28], to fine-tune LLaMA-7B [67] for commonsense reasoning tasks and save the checkpoints as the training data. We report the results across 7 sub-tasks with rank

<sup>1</sup><https://github.com/huggingface/pytorch-image-models>



rank	params. (M)	BoolQ		PIQA		SIQA		HellaSwag		ARC-e		ARC-c		OBQA	
		original	RPG	original	RPG	original	RPG	original	RPG	original	RPG	original	RPG	original	RPG
4	7.8	<b>64.3</b>	63.1	71.3	<b>72.0</b>	66.0	<b>67.5</b>	53.7	<b>56.7</b>	64.4	<b>65.3</b>	49.5	<b>49.7</b>	63.1	<b>66.0</b>
64	113.1	<b>69.3</b>	69.1	78.9	<b>79.4</b>	72.9	<b>73.9</b>	81.1	81.1	72.9	<b>73.1</b>	58.1	<b>58.3</b>	71.2	<b>72.1</b>

Table 3. Accuracy comparisons of original and generated DoRA with varying ranks for LLaMA-7B on the commonsense reasoning tasks. Our approach can generate comparable or even better results than original models. **Bold entries** are best results.

	best	avg.	min.	pos. emb.	best	avg.	min.	tokenization	best	avg.	min.	time (h)
original	75.2	74.9	74.7	learnable	<b>75.5</b>	<b>75.4</b>	<b>75.3</b>	flatten	75.3	75.2	74.8	6.2
- recurrent model	fail	fail	fail	by index	75.4	75.3	75.0	by channel	75.3	75.1	75.0	14.2
+ recurrent model	<b>75.4</b>	<b>75.3</b>	<b>75.2</b>	by layer	75.4	75.3	75.2	within layer	<b>75.4</b>	<b>75.3</b>	<b>75.2</b>	6.2

(a) Recurrent model can largely improve the performance and stability of our method.

(b) Learnable embeddings perform better, but saving cost needs to be considered.

(c) Our tokenization achieves the best trade-off between performance and training time.

Table 4. Ablation experiments of the recurrent model, position embeddings, and tokenization with ViT-Tiny on ImageNet-1K. Defaults are marked in gray. ‘fail’ indicates models performing at random-chance level. **Bold entries** are best results.

= 4 and 64 in Tab. 3. The generated models consistently yield results comparable to those of the original ones.

### 4.3. Ablation Studies and Analysis

In this section, we examine the influences of key factors on our method. We present the results of the generated ViT-Tiny [14] on the ImageNet-1K [12], unless stated otherwise.

**The effect of recurrent model.** We employ the recurrent model to learn the relationship among parameter tokens. To keep other factors consistent, we simply remove the state transition function from the recurrent model for comparison, denoted as ‘- recurrent model’. The experimental results from Tab. 4a confirm that the recurrent model plays a crucial role in parameter generation. Without the state transition function, our approach learns each parameter token individually, overlooking the relationships among these tokens. As a result, the generated parameters perform extremely poorly.

**The manner of position embeddings.** In ViT [14], the position embeddings are learnable by default. Here, we mainly conduct the experiments with three different position embedding manners and show the details as follows:

- learnable: Initializing with 2D sinusoidal positional encoding and set to be learnable.
- encoded by index: Using 1D sinusoidal positional encoding, irrespective of the original network structure, with indices assigned from front to back.
- encoded by layer (default): Using 2D sinusoidal positional encoding to represent layer and token indices.

As shown in Tab. 4b, the learnable embeddings perform slightly better than the other two manners. However, we still recommend using fixed position embeddings, as they offer comparable performance while significantly reducing storage requirements compared to the learnable position embedding scheme.

**The manner of tokenization.** Considering the differences among various layers, we divide the parameters into tokens within each layer. P-diff [69] directly flattens the parameters into 1-dimensional vectors, while SANE [61] divides the parameters by channel within each layer. We conduct experiments to analyze the 3 strategies mentioned above and compare their results in Tab. 4c. Our default strategy achieves better results than the others. Directly flattening results in a single token containing parameters from different layers, which poses challenges for optimization. Tokenizing by the channel may result in excessive padding values for each token, as the number of channels is usually much smaller than the default token size.

**The structure of recurrent model.** We mainly explore three structures of the recurrent model, including LSTM [26], Transformer [68], and Mamba [20]. In Tab. 5, we report the performances, training time, and memory cost of generating ViT-Tiny parameters on ImageNet-1K. All results are obtained on a NVIDIA H100 80G GPU. All three structures can achieve good results. However, considering the training time and memory cost, our default Mamba is the best structure of the recurrent model.

structure	best	avg.	min.	time (h)	memory (GB)
LSTM [26]	<b>75.5</b>	75.2	74.4	16.1	38.1
Transformer [68]	75.0	74.8	74.6	4.2	29.1
Mamba [19]	75.4	<b>75.3</b>	<b>75.2</b>	<b>4.1</b>	<b>27.8</b>

Table 5. We study the characteristics of three recurrent structures. Defaults are marked in gray. **Bold entries** are best results.

**Token size.** In Tab. 6, we show the results of generated ViT series with tokens of different sizes ranging from 1024 to 16384. The performance of generated models become better as the token size increases. When token is of small size, it will contain limited information that is hard to learn. De-

spite carrying large volume of information, larger token will lead to substantial memory costs (see in Appendix Fig. 8a).

model	params. (M)	token size				
		1024	2048	4096	8192	16384
ViT-Tiny	5.7	0.3	70.8	75.2	<b>75.3</b>	69.3
ViT-Small	22.1	0.1	0.7	80.5	80.5	80.4
ViT-Base	86.6	0.1	0.1	0.2	45.3	<b>84.4</b>

Table 6. Accuracy of generated models with the different token sizes. Large token size performs better on large models. **Bold entries** are best results.

**The effect of permutation state.** RPG incorporates a permutation state operation to address parameter symmetries, which become particularly pronounced when collecting checkpoints from multiple training runs. To evaluate this, we collect checkpoints from different numbers of training runs (1, 3, and 10) and compare the performance with and without permutation state. These results demonstrate that permutation state operation effectively addresses parameter symmetries and enables stable results even when incorporating checkpoints from multiple training runs.

collected runs	org.	w/o permu. state	w/ permu. state
1	88.2	88.0	88.1
3	88.3	fail	88.1
10	88.5	fail	88.2

Table 7. Permutation state effectively mitigates parameter symmetries when collecting checkpoints from different training runs.

**Efficiency of generating large-scale parameters.** Rapid synthesis of large-scale parameters is crucial for evaluating the practicality of our approach. As illustrated in Tab. 8, we present the time cost for generating models of ViT-Base and ConvNeXt-L across various DDIM [64] sampling steps. All results are obtained with a single NVIDIA H100 80G GPU. Our approach shows the capability to generate models within minutes. Notably, even for ConvNeXt-L (197.7 M parameters), we can synthesize the entire parameter within 1.3 minutes. Even with only 20 sampling steps, we can achieve promising results. Meanwhile, the inference memory requirement is approximately 20GB, so RPG can be deployed on NVIDIA RTX 3090 or similar-level GPUs.

**Similarity analysis of generated models.** In this section, we demonstrate that our method offers significant advantages over simply adding noise to the original models. Following p-diff [69], we choose Intersection of Union (IoU) as the metric for measuring similarity. It compares the agreement of output results from classification models across a large number of samples to evaluate the similarity. We calculate IoU of models from target groups with all the original

model / memory	ViT-Base / 20.7GB				ConvNeXt-L / 21.6GB			
diffusion steps	20	60	100	200	20	60	100	200
time (minute)	0.6	0.8	1.1	1.8	0.7	1.3	2.0	3.5
accuracy (%)	83.3	84.4	84.4	84.3	85.0	85.5	85.3	85.3

Table 8. GPU memory and inference time comparisons among different diffusion steps. Our approach can efficiently generate the entire ConvNeXt-L parameters (197.8 M) in minutes, requiring only  $\sim$ 20GB of GPU memory.

models and select the maximum IoU value (nearest neighbor) as the measure of similarity.

In Fig. 3, we compare original models adding various levels of noise with models generated by our method in terms of accuracy and similarity. As the noise level increases, the similarity and accuracy of the models both decreases. The points representing our generated models are distributed in the *upper left* region relative to the area with added noise, indicating that our models can enhance diversity while maintaining accuracy.

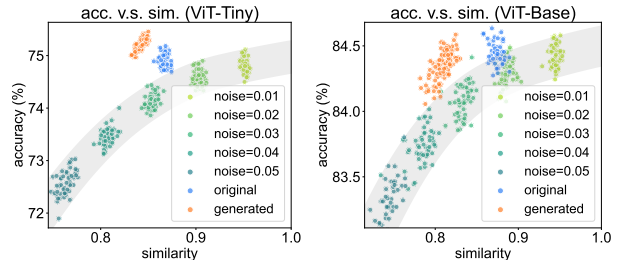


Figure 3. The figures show the trade-off between accuracy and similarity. The shaded area includes the approximate range of noise-added checkpoints. These two plots demonstrate the strong accuracy and similarity trade-off of our approach.

#### 4.4. Comparisons with Previous Methods

We compare our approach with four previous works, *i.e.*,  $S_{KDE30}$  [58], p-diff [69], D2NWG [66], and SANE [61]. As shown in Tab. 9, our approach consistently achieves the best results on various architectures, while previous works are hard to achieve comparable performances as original models. Another key issue is that the previous works usually fail to generate large-scale neural network parameters. We also provide comparisons between RPG and previous works in Tab. 10. RPG demonstrates superior capabilities in all three aspects: scalability, performance, and architecture support.

#### 5. RPG’s Potential in Unseen Tasks

Until now, experimental results have demonstrated that our approach can efficiently generate large-scale neural network parameters if these models are included in the training set. In this section, we mainly investigate whether our approach

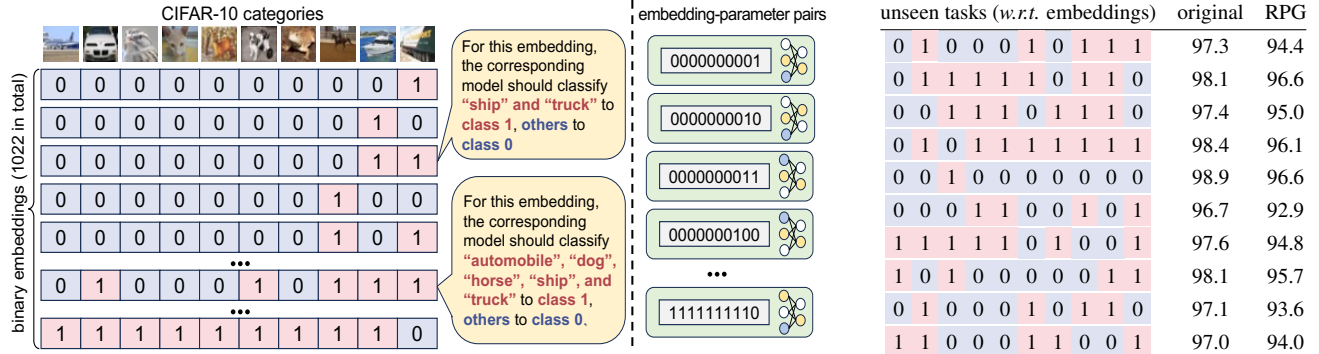


Figure 4. An illustration of our binary embedding strategy and dataset construction. Left: binary embeddings (1022 in total) encode different CIFAR-10 classification tasks, where 1s indicate classes to be classified together (e.g., ‘ship’ and ‘truck’ in the first example). Right: the dataset consists of parameter-encoding pairs, formed by network parameters with their corresponding binary embeddings. These pairs are split into non-overlapping training and validation sets.

unseen tasks (w.r.t. embeddings)	original	RPG
0 1 0 0 0 1 0 1 1 1	97.3	94.4
0 1 1 1 1 1 0 1 1 0	98.1	96.6
0 0 1 1 1 0 1 1 1 0	97.4	95.0
0 1 0 1 1 1 1 1 1 1	98.4	96.1
0 0 1 0 0 0 0 0 0 0	98.9	96.6
0 0 0 1 1 0 0 1 0 1	96.7	92.9
1 1 1 1 1 0 1 0 0 1	97.6	94.8
1 0 1 0 0 0 0 0 1 1	98.1	95.7
0 1 0 0 0 1 0 1 1 0	97.1	93.6
1 1 0 0 0 1 1 0 0 1	97.0	94.0

Table 11. Result comparisons between original and generated models on unseen embeddings (tasks). Even without seeing trained parameters of unseen tasks, RPG directly generates models that achieve competitive performance on them.

method \ model	CNN (s)	CNN (m)	MobileNetV3	ResNet-18	ViT-Base
params. (M)	0.003	0.011	4.2	11.7	86.6
original	49.0	62.1	95.4	93.9	98.7
$S_{KDE30}$ [58]	26.9	-	OOM	OOM	OOM
p-diff [69]	48.8	<u>61.9</u>	OOM	OOM	OOM
D2NWG [66]	38.2	-	82.2	-	-
SANE [61]	-	57.9	-	68.6	-
RPG	<b>49.0</b>	<b>62.0</b>	<b>89.3</b>	<b>93.6</b>	<b>98.9</b>

Table 9. Our approach obtains the best results across all architectures and largely outperforms previous works. Underline and OOM denote the reproduced results and out-of-memory issue, respectively. The detailed structures of CNN (s) and CNN (m) can be found in Model Zoos [60].

method	scalability	performance	support popular arch.
$S_{KDE30}$ [58]	✗	✗	✗
p-diff [69]	✗	✓	✗
D2NWG [66]	✓	✗	✓
SANE [61]	✓	✗	✓
RPG	✓	✓	✓

Table 10. Comparison of RPG and existing methods on key aspects: scalability to large models, effectiveness of generated parameters, and support for popular architectures. RPG excels in all three dimensions.

has the ability to generate models to tackle unseen tasks. This generalization capability is crucial as it enables RPG to handle novel tasks without requiring additional training, making it particularly valuable for real-world applications.

## 5.1. Experiment Designs.

**Build seen and unseen tasks.** To assess RPG’s capability in generating models for unseen tasks, we construct various

binary classification tasks on CIFAR-10. As illustrated in Fig. 4, we encode each task as a 10-bit binary embedding, where each bit corresponds to a CIFAR-10 category. A value of 1 indicates that the corresponding category should be classified as positive (class 1), while 0 indicates negative (class 0). For example, in the third embedding shown, ‘ship’ and ‘truck’ are assigned to class 1, while all other categories belong to class 0.

Given this encoding strategy, we can create  $2^{10}$  possible binary embeddings. After removing the two trivial cases (all 0s and all 1s), we obtain 1022 valid embeddings. For each embedding, we collect its corresponding model parameters, forming embedding-parameter pairs. These pairs are then split into *non-overlapping* sets for training and validation, allowing us to evaluate RPG’s generality on unseen tasks.

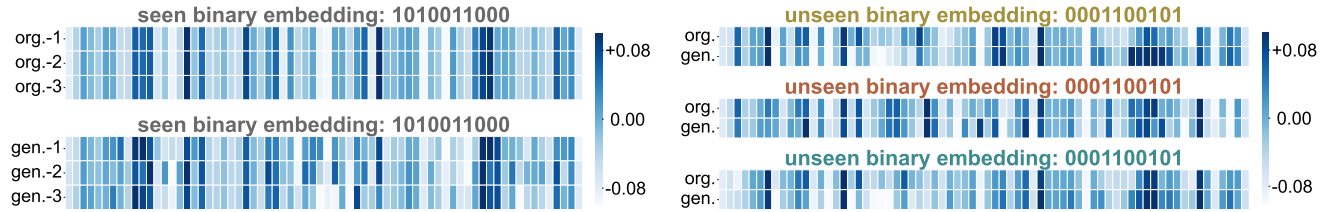
**Collection of the checkpoints.** We use ViT-Tiny to train 1022 binary classifiers on CIFAR-10 with different binary embeddings and save 3 models for each classifier. These binary embeddings serve as conditioning inputs for the subsequent RPG training process. Of these tasks, 1002 randomly selected embedding-parameter pairs serve as the training set (seen tasks), while the remaining pairs are reserved as unseen tasks for evaluation.

**Training of RPG.** We only use the 1002 checkpoints from seen tasks to train RPG. Meanwhile, these embeddings are also fed into RPG as conditional inputs of the recurrent model. During the training stage, the checkpoints trained by the unseen binary embeddings are not accessible.

**Evaluation details.** We input the unseen binary embeddings to the trained RPG to generate the parameters for unseen tasks. The results of the original and generated unseen models are reported for comparison.

binary embedding (from seen set)	1	0	1	1	1	0	1	0	0	0
accuracy (%)	98.0	99.1	98.5	94.4	98.1	92.2	99.2	97.0	97.1	99.1
flipped embedding (from unseen set)	0	1	0	0	0	1	0	1	1	1
accuracy (%)	92.3	98.9	94.0	85.4	92.2	90.8	99.3	95.3	97.6	98.1

Table 12. Result comparisons of binary embedding change. The accuracy in the table is for each individual class. RPG can be aware of such change accurately. More results can be found in Appendix B.4.



(a) Original and generated models with identical seen binary embeddings are compared. The three original models exhibit homogeneity, while the generated models display diversity.

(b) Original and generated models with 3 unseen binary embeddings are compared. The results confirm that our approach can learn high-performing parameter patterns even when they are not included in the training set.

Figure 5. Illustration of the parameters of original and generated models in seen and unseen embeddings. We select 100 parameters of the classification head and visualize its normalized values.

## 5.2. Results for Unseen Tasks

**Performance comparisons.** We compare the results of our approach and original models on unseen binary embeddings in Tab. 11. Considering the space limitation, we randomly select 10 unseen binary embeddings for comparison. Notably, RPG yields commendable performance in these unseen tasks, even without being trained on the specific unseen embeddings. That demonstrates the strong practicality and potential of our approach in generating models under unseen tasks. The results of the remaining unseen binary embeddings and more analysis are shown in Appendix B.4.

**Perception of embedding changes.** In addition to comparing results, we further investigate our approach’s ability to perceive embedding changes. We select two tasks with opposite binary embeddings in each element and report the results in Tab. 12. Our approach demonstrates a remarkable capacity to accurately detect changes in the tasks and generate corresponding model parameters. It is worth noting that the accuracy would hover around 50% if our approach were not aware of the embedding changes.

**Visualizations of original and generated model parameters.** We visualize the original and generated models for both seen and unseen tasks in Fig. 5. For seen tasks, our approach generates diverse models compared to the original ones. Surprisingly, as shown in Fig. 5b, we find that our approach can learn unseen parameter patterns. This demonstrates the potential generalization ability of our method.

**Efficiency comparison.** To evaluate efficiency on unseen tasks, we compare 3 approaches: i) training ViT-Tiny from scratch, ii) finetuning an ImageNet-pretrained ViT-Tiny, and iii) finetuning a RPG-initialized model. As shown in

epoch	from scratch	finetune	RPG initialization + finetune
0	50.0	52.9	94.4
1	61.4	90.3	96.8
5	69.1	96.3	97.3
10	74.9	97.1	97.5
50	86.7	97.7	97.8

Table 13. Accuracy (%) comparison for different training strategies on an unseen task. RPG initialization demonstrates superior performance and faster convergence.

Tab. 13, RPG significantly accelerates training for the unseen task. These results establish RPG initialization as an effective approach that significantly reduces training costs.

## 6. Discussion and Conclusion

Our approach demonstrates promising results in large-scale parameter generation across various vision and language tasks. However, we acknowledge that achieving true ‘AI creating AI’ remains a distant goal. Firstly, while our method shows potential in generating models for unseen tasks, it currently faces limitations in generating parameters for novel model architectures. Secondly, our approach is constrained by modeling parameter relationships within a single task, potentially limiting its practical applicability. More importantly, future work should focus on simultaneously modeling parameter relationships across diverse architectures and tasks. Such an approach could yield a more powerful and versatile parameter generator, potentially advancing us closer to the ‘AI creating AI’ era. We hope our approach will inspire future research in this field.

**Acknowledgments.** We sincerely thank Zhiyuan Liang,



Gongfan Fang, Xuanlei Zhao, Zangwei Zheng, Ziheng Qin, Tianlong Chen, and Zhangyang Wang for valuable discussions and feedbacks. This research is supported by the National Research Foundation, Singapore under its AI Singapore Programme (AISG Award No: AISG2-PhD-2021-08-008).

## References

- [1] Vijay Badrinarayanan, Bamdev Mishra, and Roberto Cipolla. Understanding symmetries in deep networks. *arXiv*, 2015. 3
- [2] Maximilian Beck, Korbinian Pöppel, Markus Spanring, Andreas Auer, Oleksandra Prudnikova, Michael Kopp, Günter Klambauer, Johannes Brandstetter, and Sepp Hochreiter. xlstm: Extended long short-term memory. *arXiv preprint arXiv:2405.04517*, 2024. 2
- [3] Yonatan Bisk, Rowan Zellers, Jianfeng Gao, Yejin Choi, et al. Piqa: Reasoning about physical commonsense in natural language. In *AAAI*, pages 7432–7439, 2020. 4, 13
- [4] Charles Blundell, Julien Cornebise, Koray Kavukcuoglu, and Daan Wierstra. Weight uncertainty in neural network. In *ICML*. PMLR, 2015. 2
- [5] Léon Bottou et al. Stochastic gradient learning in neural networks. *Proceedings of Neuro-Nimes*, 91(8), 1991. 2
- [6] Andrew Brock, Theo Lim, J.M. Ritchie, and Nick Weston. SMASH: One-shot model architecture search through hypernetworks. In *ICLR*, 2018. 2
- [7] Krzysztof Choromanski, Valerii Likhoshesterov, David Dohan, Xingyou Song, Andreea Gane, Tamas Sarlos, Peter Hawkins, Jared Davis, Afroz Mohiuddin, Lukasz Kaiser, et al. Rethinking attention with performers. *arXiv preprint arXiv:2009.14794*, 2020. 2
- [8] Gene Chou, Yuval Bahat, and Felix Heide. Diffusion-sdf: Conditional generative modeling of signed distance functions. In *ICCV*, pages 2262–2272, 2023. 2
- [9] Christopher Clark, Kenton Lee, Ming-Wei Chang, Tom Kwiatkowski, Michael Collins, and Kristina Toutanova. Boolq: Exploring the surprising difficulty of natural yes/no questions. *arXiv preprint arXiv:1905.10044*, 2019. 4, 13
- [10] Peter Clark, Isaac Cowhey, Oren Etzioni, Tushar Khot, Ashish Sabharwal, Carissa Schoenick, and Oyvind Tafjord. Think you have solved question answering? try arc, the ai2 reasoning challenge. *arXiv preprint arXiv:1803.05457*, 2018. 4, 13
- [11] Tri Dao and Albert Gu. Transformers are ssm: Generalized models and efficient algorithms through structured state space duality. *arXiv preprint arXiv:2405.21060*, 2024. 2
- [12] Jia Deng, Wei Dong, Richard Socher, Li-Jia Li, Kai Li, and Li Fei-Fei. Imagenet: A large-scale hierarchical image database. In *CVPR*, pages 248–255. Ieee, 2009. 4, 5, 13
- [13] Prafulla Dhariwal and Alexander Nichol. Diffusion models beat gans on image synthesis. In *NeurIPS*, pages 8780–8794, 2021. 2
- [14] Alexey Dosovitskiy, Lucas Beyer, Alexander Kolesnikov, Dirk Weissenborn, Xiaohua Zhai, Thomas Unterthiner, Mostafa Dehghani, Matthias Minderer, Georg Heigold, Sylvain Gelly, Jakob Uszkoreit, and Neil Houlsby. An image is worth 16x16 words: Transformers for image recognition at scale. In *ICLR*, 2021. 1, 2, 3, 4, 5
- [15] Ziya Erkoç, Fangchang Ma, Qi Shan, Matthias Nießner, and Angela Dai. Hyperdiffusion: Generating implicit neural fields with weight-space diffusion. In *ICCV*, 2023. 2
- [16] Gongfan Fang, Xinyin Ma, and Xinchao Wang. Structural pruning for diffusion models. In *NeurIPS*, 2023. 2
- [17] Yarin Gal and Zoubin Ghahramani. Dropout as a bayesian approximation: Representing model uncertainty in deep learning. In *ICML*. PMLR, 2016. 2
- [18] Alex Graves. Practical variational inference for neural networks. *NeurIPS*, 24, 2011. 2
- [19] Albert Gu and Tri Dao. Mamba: Linear-time sequence modeling with selective state spaces. *arXiv preprint arXiv:2312.00752*, 2023. 2, 5, 13
- [20] Albert Gu and Tri Dao. Mamba: Linear-time sequence modeling with selective state spaces. *arXiv preprint arXiv:2312.00752*, 2024. 3, 4, 5
- [21] David Ha, Andrew M. Dai, and Quoc V. Le. Hypernetworks. In *ICLR*, 2017. 1, 2
- [22] Kaiming He, Xiangyu Zhang, Shaoqing Ren, and Jian Sun. Deep residual learning for image recognition. In *CVPR*, pages 770–778, 2016. 1, 2, 4
- [23] Jonathan Ho, Ajay Jain, and Pieter Abbeel. Denoising diffusion probabilistic models. In *NeurIPS*, pages 6840–6851, 2020. 2
- [24] Sepp Hochreiter. Untersuchungen zu dynamischen neuronalen netzen. *Diploma, Technische Universität München*, 91(1):31, 1991. 2
- [25] S Hochreiter. Long short-term memory. *Neural Computation MIT-Press*, 1997. 2
- [26] Sepp Hochreiter, Sepp Schmidhuber Jürgen, Hochreiter, and Schmidhuber. Long short-term memory. *Neural Comput.*, 9 (8):1735–1780, 1997. 3, 5
- [27] Edward J Hu, Yelong Shen, Phillip Wallis, Zeyuan Allen-Zhu, Yuanzhi Li, Shean Wang, Lu Wang, and Weizhu Chen. Lora: Low-rank adaptation of large language models. *arXiv preprint arXiv:2106.09685*, 2021. 2
- [28] Edward J Hu, yelong shen, Phillip Wallis, Zeyuan Allen-Zhu, Yuanzhi Li, Shean Wang, Lu Wang, and Weizhu Chen. LoRA: Low-rank adaptation of large language models. In *ICLR*, 2022. 4
- [29] Xiaolong Jin, Kai Wang, Dongwen Tang, Wangbo Zhao, Yukun Zhou, Junshu Tang, and Yang You. Conditional lora parameter generation. *arXiv preprint arXiv:2408.01415*, 2024. 2, 4
- [30] Diederik P Kingma and Max Welling. Auto-encoding variational bayes. *arXiv preprint arXiv:1312.6114*, 2013. 2
- [31] Durk P Kingma, Tim Salimans, and Max Welling. Variational dropout and the local reparameterization trick. In *NeurIPS*, 2015. 2
- [32] Alex Krizhevsky and Geoffrey Hinton. Learning multiple layers of features from tiny images. Technical report, University of Toronto, 2009. 1, 13

- [33] Alex Krizhevsky, Ilya Sutskever, and Geoffrey E Hinton. Imagenet classification with deep convolutional neural networks. In *NeurIPS*, 2012. 1
- [34] Daniel Kunin, Javier Sagastuy-Brena, Surya Ganguli, Daniel LK Yamins, and Hidenori Tanaka. Neural mechanics: Symmetry and broken conservation laws in deep learning dynamics. In *ICLR*, 2021. 3
- [35] Tianhong Li, Yonglong Tian, He Li, Mingyang Deng, and Kaiming He. Autoregressive image generation without vector quantization. *arXiv preprint arXiv:2406.11838*, 2024. 3
- [36] Yanghao Li, Hanzi Mao, Ross Girshick, and Kaiming He. Exploring plain vision transformer backbones for object detection. In *ECCV*, pages 280–296. Springer, 2022. 4
- [37] Zexi Li, Lingzhi Gao, and Chao Wu. Text-to-model: Text-conditioned neural network diffusion for train-once-for-all personalization. *arXiv preprint arXiv:2405.14132*, 2024. 2
- [38] Lequan Lin, Dai Shi, Andi Han, Zhiyong Wang, and Junbin Gao. Unleash graph neural networks from heavy tuning. *arXiv preprint arXiv:2405.12521*, 2024. 2
- [39] Tsung-Yi Lin, Michael Maire, Serge Belongie, James Hays, Pietro Perona, Deva Ramanan, Piotr Dollár, and C Lawrence Zitnick. Microsoft coco: Common objects in context. In *Computer Vision—ECCV 2014: 13th European Conference, Zurich, Switzerland, September 6–12, 2014, Proceedings, Part V 13*, pages 740–755. Springer, 2014. 4, 13
- [40] Shih-Yang Liu, Chien-Yi Wang, Hongxu Yin, Pavlo Molchanov, Yu-Chiang Frank Wang, Kwang-Ting Cheng, and Min-Hung Chen. Dora: Weight-decomposed low-rank adaptation. *arXiv preprint arXiv:2402.09353*, 2024. 4
- [41] Zhuang Liu, Hanzi Mao, Chao-Yuan Wu, Christoph Feichtenhofer, Trevor Darrell, and Saining Xie. A convnet for the 2020s. In *CVPR*, pages 11976–11986, 2022. 2, 4
- [42] Cheng Lu, Yuhao Zhou, Fan Bao, Jianfei Chen, Chongxuan Li, and Jun Zhu. Dpm-solver: A fast ode solver for diffusion probabilistic model sampling in around 10 steps. In *NeurIPS*, pages 5775–5787, 2022. 2
- [43] Xinyin Ma, Gongfan Fang, and Xinchao Wang. Deepcache: Accelerating diffusion models for free. In *CVPR*, pages 15762–15772, 2024. 2
- [44] AI Meta. Introducing meta llama 3: The most capable openly available llm to date. *Meta AI*, 2024. 1
- [45] Todor Mihaylov, Peter Clark, Tushar Khot, and Ashish Sabharwal. Can a suit of armor conduct electricity? a new dataset for open book question answering. In *EMNLP*, 2018. 13
- [46] Noboru Murata, Shuji Yoshizawa, and Shun-ichi Amari. Network information criterion-determining the number of hidden units for an artificial neural network model. *IEEE transactions on neural networks*, 5(6), 1994. 2
- [47] Radford M Neal. *Bayesian learning for neural networks*. Springer Science & Business Media, 2012. 2
- [48] Alexander Quinn Nichol and Prafulla Dhariwal. Improved denoising diffusion probabilistic models. In *ICML*, pages 8162–8171. PMLR, 2021. 2
- [49] Zizheng Pan, Bohan Zhuang, De-An Huang, Weili Nie, Zhiding Yu, Chaowei Xiao, Jianfei Cai, and Anima Anandkumar. T-stitch: Accelerating sampling in pre-trained diffusion models with trajectory stitching. *arXiv preprint arXiv:2402.14167*, 2024. 2
- [50] William Peebles and Saining Xie. Scalable diffusion models with transformers. In *ICCV*, pages 4195–4205, 2023. 2
- [51] William Peebles, Ilija Radosavovic, Tim Brooks, Alexei A Efros, and Jitendra Malik. Learning to learn with generative models of neural network checkpoints. *arXiv preprint arXiv:2209.12892*, 2022. 1, 2, 4, 12
- [52] Bo Peng, Eric Alcaide, Quentin Anthony, Alon Albalak, Samuel Arcadinho, Stella Biderman, Huanqi Cao, Xin Cheng, Michael Chung, Matteo Grella, et al. Rkv: Reinventing rnns for the transformer era. *arXiv preprint arXiv:2305.13048*, 2023. 2
- [53] Alec Radford. Improving language understanding by generative pre-training. 2018. 2
- [54] Danilo Jimenez Rezende, Shakir Mohamed, and Daan Wierstra. Stochastic backpropagation and approximate inference in deep generative models. In *ICML*. PMLR, 2014. 2
- [55] Robin Rombach, Andreas Blattmann, Dominik Lorenz, Patrick Esser, and Björn Ommer. High-resolution image synthesis with latent diffusion models. In *CVPR*, pages 10684–10695, 2022. 2
- [56] Maarten Sap, Hannah Rashkin, Derek Chen, Ronan LeBras, and Yejin Choi. Socialliqa: Commonsense reasoning about social interactions. *arXiv preprint arXiv:1904.09728*, 2019. 4, 13
- [57] Wouter F Schmidt, Martin A Kraaijveld, Robert PW Duin, et al. Feed forward neural networks with random weights. In *ICPR*. IEEE Computer Society Press, 1992. 2
- [58] Konstantin Schürholt, Boris Knyazev, Xavier Giró-i Nieto, and Damian Borth. Hyper-representations as generative models: Sampling unseen neural network weights. In *NeurIPS*, pages 27906–27920, 2022. 2, 6, 7, 12, 16, 17
- [59] Konstantin Schürholt, Boris Knyazev, Xavier Giró-i Nieto, and Damian Borth. Hyper-representations for pre-training and transfer learning. *arXiv preprint arXiv:2207.10951*, 2022. 2, 12
- [60] Konstantin Schürholt, Diyar Taskiran, Boris Knyazev, Xavier Giró-i Nieto, and Damian Borth. Model zoos: A dataset of diverse populations of neural network models. In *NeurIPS*, 2022. 7, 12
- [61] Konstantin Schürholt, Michael W Mahoney, and Damian Borth. Towards scalable and versatile weight space learning. *arXiv preprint arXiv:2406.09997*, 2024. 2, 5, 6, 7, 12
- [62] Junhyuk So, Jungwon Lee, Daehyun Ahn, Hyungjun Kim, and Eunhyeok Park. Temporal dynamic quantization for diffusion models. In *NeurIPS*, 2024. 2
- [63] Haim Sompolinsky, Andrea Crisanti, and Hans-Jurgen Sommers. Chaos in random neural networks. *Physical review letters*, 61(3), 1988. 2
- [64] Jiaming Song, Chenlin Meng, and Stefano Ermon. Denoising diffusion implicit models. *arXiv preprint arXiv:2010.02502*, 2020. 2, 6
- [65] Yang Song, Prafulla Dhariwal, Mark Chen, and Ilya Sutskever. Consistency models. *arXiv preprint arXiv:2303.01469*, 2023. 2

- [66] Bedionita Soro, Bruno Andreis, Hayeon Lee, Song Chong, Frank Hutter, and Sung Ju Hwang. Diffusion-based neural network weights generation. *arXiv preprint arXiv:2402.18153*, 2024. [1](#), [2](#), [4](#), [6](#), [7](#)
- [67] Hugo Touvron, Thibaut Lavril, Gautier Izacard, Xavier Martinet, Marie-Anne Lachaux, Timothée Lacroix, Baptiste Rozière, Naman Goyal, Eric Hambro, Faisal Azhar, et al. Llama: Open and efficient foundation language models. *arXiv preprint arXiv:2302.13971*, 2023. [2](#), [4](#)
- [68] A Vaswani. Attention is all you need. In *NeurIPS*, 2017. [2](#), [3](#), [5](#)
- [69] Kai Wang, Zhaopan Xu, Yukun Zhou, Zelin Zang, Trevor Darrell, Zhuang Liu, and Yang You. Neural network diffusion. *arXiv preprint arXiv:2402.13144*, 2024. [1](#), [2](#), [3](#), [4](#), [5](#), [6](#), [7](#), [12](#), [13](#), [16](#)
- [70] Sinong Wang, Belinda Z Li, Madian Khabsa, Han Fang, and Hao Ma. Linformer: Self-attention with linear complexity. *arXiv preprint arXiv:2006.04768*, 2020. [2](#)
- [71] Eugene Wong. Stochastic neural networks. *Algorithmica*, 6 (1-6), 1991. [2](#)
- [72] Tete Xiao, Yingcheng Liu, Bolei Zhou, Yuning Jiang, and Jian Sun. Unified perceptual parsing for scene understanding. In *ECCV*, pages 418–434, 2018. [4](#)
- [73] An Yang, Baosong Yang, Binyuan Hui, Bo Zheng, Bowen Yu, Chang Zhou, Chengpeng Li, Chengyuan Li, Dayiheng Liu, Fei Huang, Guanting Dong, Haoran Wei, Huan Lin, Jialong Tang, Jialin Wang, Jian Yang, Jiahong Tu, Jianwei Zhang, Jianxin Ma, Jin Xu, Jingren Zhou, Jinze Bai, Jinzheng He, Junyang Lin, Kai Dang, Keming Lu, Keqin Chen, Kexin Yang, Mei Li, Mingfeng Xue, Na Ni, Pei Zhang, Peng Wang, Ru Peng, Rui Men, Ruize Gao, Runji Lin, Shijie Wang, Shuai Bai, Sinan Tan, Tianhang Zhu, Tianhao Li, Tianyu Liu, Wenbin Ge, Xiaodong Deng, Xiaohuan Zhou, Xingzhang Ren, Xinyu Zhang, Xipin Wei, Xuancheng Ren, Yang Fan, Yang Yao, Yichang Zhang, Yu Wan, Yunfei Chu, Yuqiong Liu, Zeyu Cui, Zhenru Zhang, and Zhihao Fan. Qwen2 technical report. *arXiv preprint arXiv:2407.10671*, 2024. [15](#)
- [74] Xingyi Yang, Daquan Zhou, Jiashi Feng, and Xinchao Wang. Diffusion probabilistic model made slim. In *CVPR*, pages 22552–22562, 2023. [2](#)
- [75] Rowan Zellers, Ari Holtzman, Yonatan Bisk, Ali Farhadi, and Yejin Choi. Hellaswag: Can a machine really finish your sentence? *arXiv preprint arXiv:1905.07830*, 2019. [4](#), [13](#)
- [76] Wangbo Zhao, Jiasheng Tang, Yizeng Han, Yibing Song, Kai Wang, Gao Huang, Fan Wang, and Yang You. Dynamic tuning towards parameter and inference efficiency for vit adaptation. *arXiv preprint arXiv:2403.11808*, 2024. [4](#)
- [77] Bolei Zhou, Hang Zhao, Xavier Puig, Sanja Fidler, Adela Barriuso, and Antonio Torralba. Scene parsing through ade20k dataset. In *CVPR*, 2017. [4](#), [13](#)

We organize our appendix as follows.

### Discussion with More Related Works

- Section A.1 Discussion with HyperRepresentations.
- Section A.2 Details and limitations of G.pt.
- Section A.3 Details and limitations of p-diff.

### Experimental Settings and More Results

- Section B.1: Training recipe.
- Section B.2: Datasets.
- Section B.3: The detailed structure of recurrent diffusion.
- Section B.4: More results of Section 5.
- Section B.5: Training memory cost analysis.
- Section B.6: Inference memory cost and sampling time.
- Section B.7: Parameter sensitivity v.s. performance.
- Section B.8: Why not auto-regression?

## A. Discussion with More Related Works

### A.1. Discussion with HyperRepresentations.

We mainly compare with three HyperRepresentation methods [58, 59, 61]. These methods use an autoencoder to learn the latent features of trained models, so they call the latent feature HyperRepresentation. This HyperRepresentation is then used for analyzing the model’s performance or characteristics, or for sampling to generate new models or pre-trained parameters.

- [58] utilizes kernel density estimation (KDE) to sample model parameters on the learned HyperRepresentation space. They also emphasize the importance of layer-wise loss normalization in the learning process of HyperRepresentation. This work achieves parameter generation in small CNNs from Model Zoos [60] with 2864 parameters.
- [59] focuses on using HyperRepresentation to sample the pre-trained model parameters. They also evaluate the ability of transfer learning by using a trained parameter autoencoder to initialize on unseen dataset. This work can be regarded as a cheap parameter initialization method.
- [61] utilizes a sequential autoencoder for neural embeddings (SANE) to divide the neural network weights into subsets. Then, an autoencoder processes these subsets in a sliding window. This work can generate the entire parameter of ResNet-18. However, the performance of generated ResNet-18 is poor and exists a large gap with the original trained ResNet-18. For example, the performance of generated ResNet-18 is 68.6%, while the original model can achieve an accuracy of over 90% on CIFAR-10 (see in Tab. 9).

We summarize the main differences as follows:

- *Hyper-representations as generative models* is hard to achieve comparable results as their original models that are used for training, but our approach obtains comparable results.
- *Hyper-representation for pre-training and transfer learn-*

*ing* focuses on parameter initialization while our approach targets to learn the distribution of high-performing neural network parameters.

- *SANE* is the latest method among these three HyperRepresentation methods. However, SANE uses a sliding window to model the relationship of a small part of trained parameters. Our approach uses a recurrent model among all parameters.
- Our approach can synthesize many popular vision and language parameters, such as ConvNeXt-L and LoRA parameters of LLaMA-7B, with a maximum parameter count of approximately 200M, which is much larger than previous works.

Additionally, the parameters generated by our model can directly achieve almost peak performance without any finetuning. And the generation process is entirely synthesized from noise, eliminating the need for a few prompt examples that are trained for a few epochs, as required by the  $S_{\text{KDE}}$  [61] sampling method.

The capability of large-scale and high-accuracy generation makes our method more applicable in practical scenarios, significantly bridging the gap between theoretical parameter generation and practical application.

### A.2. Details and limitations of G.pt.

A primary limitation of G.pt [51] is the training data collection cost. By default, they collect 23 million checkpoints to train the parameter generator. Besides, they only evaluate the effectiveness of G.pt on small architectures, such as a low-dimensional MLP layer or a Convolutional layer with limited channels. The maximum number of generated parameters does not exceed 10,000.

### A.3. Details and limitations of p-diff.

P-diff [69] directly flattens all parameters into a single-dimensional vector, disregarding the inter-layer parameter relationships. Furthermore, p-diff faces challenges in scaling up to large-scale parameter generation.

## B. Experimental Settings and More Results

### B.1. Training recipe

In this section, we provide detailed training recipes and supplementary information. The number of parameters generated by our approach ranges from approximately 3K to 200M. The significant disparity necessitates different training settings. Generally, as the number of parameters increases, the learning process becomes more challenging, requiring higher training costs, particularly for generating parameters beyond 50 million. Therefore, our training settings are divided into two categories: the default setting and the setting for parameters exceeding 50 million, as is shown in Tab. 14.



**Data parallelism:** When the number of parameters is less than 50 million, we adopt a single GPU to run the training process. For larger number of parameters, we employ distributed data parallelism to facilitate the training.

**Diffusion batch size:** In our approach, the diffusion model is shared across all tokens. Typically, all tokens can be fed as a single batch into the diffusion model for training. However, in practice, we randomly select a subset of tokens from a long sequence for training, rather than feeding all parts at once. This approach significantly reduces memory usage without compromising performance. The “diffusion batch size” in Tab. 14 refers to the number of tokens fed into the diffusion model during a single training iteration.

training setting	params. count < 50M	params. count > 50M
batch size	16	8
optimizer	AdamW	AdamW
learning rate	3e-5	1e-5
training steps	80,000	120,000
weight decay	1e-5	1e-5
mixed precision	bfloat16	bfloat16
diffusino batch size	1024	512

Table 14. Training recipe in detail. The amount of parameters that need to be generated is denoted as *params. count*

## B.2. Datasets

In this section, we introduce the datasets used in the paper, including those for classification, semantic segmentation, object detection&instance segmentation, and commonsense reasoning.

### Classification

- **ImageNet-1k** [12] is a large-scale visual database for visual object recognition research. It contains over 1 million images across 1000 categories and is widely used for training and benchmarking deep learning models.
- **CIFAR-10** [32] dataset consists of 60,000  $32 \times 32$  colorful images in 10 different classes. It is commonly used for training machine learning and computer vision algorithms, providing a standard benchmark for image classification task.

### Semantic segmentation

- **ADE20K** [77] is a dataset for semantic segmentation and scene parsing, containing over 20,000 images annotated with pixel-level labels for 150 object categories. It is used to train models to understand and segment various objects and scenes in an image, making it valuable for applications in autonomous driving, robotics, and image editing.

### Instance segmentation & Object detection

- **COCO** [39] dataset is a large-scale object detection, segmentation, and captioning dataset. It contains over 330,000 images, with more than 200,000 labeled instances across 80 object categories. COCO is widely

used for training and evaluating models in object detection, segmentation, and image captioning tasks.

### Commonsense reasoning:

- **BoolQ** [9]: Yes/no questions based on natural passages.
- **PIQA** [3]: Questions about physical tasks and actions.
- **SIQA** [56]: Questions about social interactions.
- **HellaSwag** [75]: Choosing the correct ending for stories.
- **ARC** [10]: Multiple-choice science questions.
- **OBQA** [45]: Questions requires multi-step reasoning, commonsense knowledge, and rich text comprehension.

## B.3. The detailed structure of recurrent diffusion

In this section, we provide specific details about the proposed recurrent model and diffusion model in RPG. More detailed configurations can be found in Tab. 15.

**Details of recurrent model.** By default, the recurrent model consists of two Mamba layers [19]. As the increasing of parameters to generate, we need a larger recurrent model to capture the information in these parameters. The size of the recurrent model is mainly determined by the token size, which varies according to the number of parameters to be generated. Based on the token size, we categorize our model into four versions: Tiny, Small, Base, and Large.

**Details of diffusion model.** Following p-diff [69], our diffusion model adopts a one-dimensional convolutional architecture. The parameters of the diffusion model are significantly fewer than those of the recurrent model. We feed the prototypes from the recurrent model as conditions into the diffusion model by directly adding them to the feature map.

## B.4. More results of Section 5

**Results of generating models for unseen tasks.** In Section 5, we show the potential of our approach in generating models for unseen tasks. In this part, we provide more results. First, we compare the performance of original and generated models using all unseen embeddings in Tab. 16. Results demonstrate that our approach consistently achieves good results in unseen tasks.

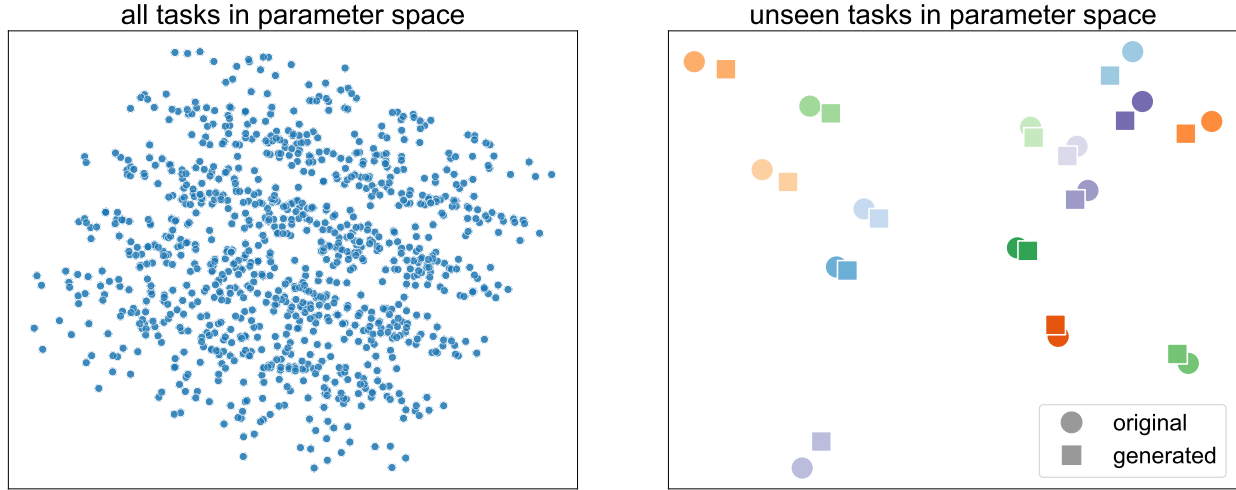
**PCA visualization of classification head parameters.** We also provide a visualization of the parameters of the classification head (a two-layer fully connected structure with total 38,976 parameters) for 1022 tasks as described in Section 5 using Principal Component Analysis (PCA), which presents the structure of the parameter space in Fig. 6a. Our generated model achieves an average accuracy of 91.2% across all binary classification tasks, which indicates that our method has effectively learned this structure. Furthermore, we evaluate the parameters corresponding to unseen tasks and compared their positions in Fig. 6b between the original and generated parameters. It is noteworthy that, even though the original parameters of these tasks are not included in the training data, the generated parameters con-

module	setting	RPG-Tiny	RPG-Small	RPG-Base	RPG-Large
adequate number of parameters		<50K	50K~10M	5M~50M	>50M
recurrent (Mamba)	d_model of 1st layer	256	4096	8192	12288
	d_model of 2nd layer	256	4096	8192	16384
	d_state	32	128	128	128
	d_conv	4	4	4	4
	expand	2	2	2	2
	parameter counts	1.3M	256M	1018M	3076M
diffusion (1D CNN)	encoder channels	(1, 32, 64, 128)	(1, 32, 64, 128)	(1, 32, 64, 128)	(1, 64, 96)
	decoder channels	(128, 64, 32, 1)	(128, 64, 32, 1)	(128, 64, 32, 1)	(96, 64, 1)
	token size	256	4096	8192	16384
	kernel size	7	7	7	7
	default solver	DDPM	DDPM	DDPM	DDIM
	sampling steps	1000	1000	1000	60
	$\beta$ -start & $\beta$ -end	(0.0001, 0.02)	(0.0001, 0.02)	(0.0001, 0.02)	(0.0001, 0.02)
	betas schedule	linear	linear	linear	linear
	number time steps	1000	1000	1000	1000
	parameter counts	0.3M	17M	69M	273M

Table 15. Detailed information about four different sizes of recurrent diffusion. The *adequate number of parameters* implies that our model is usually adequate to generate parameters in that scale, which is empirical results instead of an exact rule. It also necessitates considering other factors such as parameter sensitivity.

unseen binary embeddings	original	best acc.	average acc.	standard deviation
0 1 0 0 0 1 0 1 1 1	97.3	94.4	93.9	0.6
0 1 1 1 1 1 0 1 1 0	98.1	96.6	94.9	2.1
0 0 1 1 1 0 1 1 1 0	97.4	95.0	94.2	1.1
0 1 0 1 1 1 1 1 1 1	98.4	96.1	95.8	0.3
0 0 1 0 0 0 0 0 0 0	98.9	96.6	95.2	2.3
0 0 0 1 1 0 0 1 0 1	96.7	92.9	91.6	1.1
1 1 1 1 1 0 1 0 0 1	97.6	94.8	94.1	0.7
1 0 1 0 0 0 0 0 1 1	98.1	95.7	91.8	3.7
0 1 0 0 0 1 0 1 1 0	97.1	93.6	90.7	4.3
1 1 0 0 0 1 1 0 0 1	97.0	94.0	90.1	3.6
1 0 1 0 0 0 1 1 0 1	97.3	91.3	90.7	0.8
0 1 1 1 1 0 0 0 1 0	96.3	95.4	89.4	6.3
1 1 0 1 1 1 0 1 0 0	97.6	92.6	90.5	3.2
0 1 1 1 0 0 1 1 1 0	96.3	90.8	89.1	1.9
0 1 0 0 1 1 1 0 1 0	96.3	91.9	88.4	4.4
0 0 1 0 0 0 1 1 0 1	97.5	93.7	88.0	5.6
0 0 0 1 1 0 1 1 1 1	96.5	90.8	85.5	7.0
1 0 0 1 0 0 1 1 0 1	96.4	86.7	83.7	3.6
1 0 0 1 0 1 0 0 0 0	97.7	85.6	83.2	2.0
0 0 1 1 0 0 0 1 0 1	96.3	90.2	79.2	9.6

Table 16. Performance comparisons between original and generated models on unseen tasks. Specifically, we generated 10 models for each unseen task, with binary embeddings in the unseen set as condition. The results consistently show that our generated models perform comparably to the original models.



(a) Visualization of the classification head of all 1022 tasks. This reveals that there is an inherent structure among the high-dimensional parameters, which can be captured by deep learning models.

(b) Visualization of the classification head in some unseen tasks. Parameters associated with the same task are indicated by a consistent color. Our method can capture the structure of the parameter space.

Figure 6. Principal Component Analysis (PCA) visualization of the classification head. The figures demonstrate the presence of an inherent structure in the high-dimensional parameter space and highlight our method’s effectiveness in capturing this structure for unseen tasks.

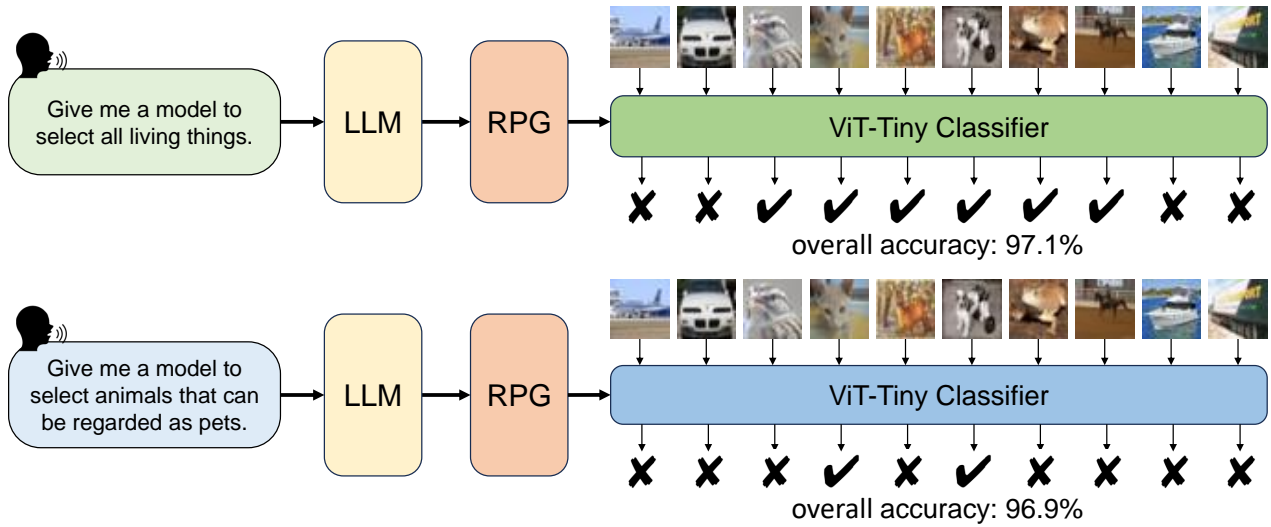


Figure 7. Examples of RPG-generated models guided by binary embeddings from a large language model (Qwen2.5-3B [73]), demonstrating neural network parameter generation conditioned by natural language. For the first example, we give the LLM a prompt: "Give me a model to select all living things." With the binary embedding provided by the LLM, our RPG then generates a ViT-Tiny classifier. After that, We use images in CIFAR-10 to evaluate the model’s accuracy. The model should classify "bird", "cat", "deer", "dog", "frog", and "horse" to the positive class, which we used as the ground truth. The result is 97.1%. The second example follows the same process.

sistently appeared in close proximity to the original ones. This observation further highlights the capability of our method to model the structure of the parameter space, even for tasks not previously encountered.

**Conditional generation guided by LLM.** To demonstrate the application scenarios of our model, we utilize large lan-

guage model to generate binary embeddings to guide RPG in generating corresponding classification models. We provide two example results in Fig. 7. This experiment demonstrates our method’s capability to generate neural network parameters based on natural language guidance, highlighting the potential applications of our method.

## B.5. Training memory cost analysis

In this section, we analyze the GPU memory utilization during training. GPU memory consumption is usually highly correlated with two factors: i) the size of the generative model and ii) the size of generated parameters. We analyzed the impact of these two factors on the GPU memory utilization during the training of our approach.

**GPU memory v.s. token size** We visualize the GPU memory usage with different token sizes in Fig. 8a. As the token size increases, the scale of the recurrent model significantly grows, leading to a notable increase in GPU memory consumption. This implies that, when the performance of the generated models is comparable, we prefer to use models with smaller token sizes.

**GPU memory v.s. parameter counts** We conduct experiments to show the relationship between GPU memory and generated parameter counts in Fig. 8b. In previous methods, the relationship between GPU memory consumption and the number of parameters in the generated model was quadratic [58] or directly proportional [69]. This limits their practicality and application range. In contrast, our approach demonstrates remarkable efficiency: with equivalent GPU memory usage, it can generate models with 34 to 960 times more parameters compared to previous methods.

## B.6. Inference memory cost and sampling time

In this section, we present more information about the sampling, including memory usage, inference time, and the balance between sequential and parallel inference. In Tab. 8, we show the sampling time and memory usage for ViT-Base and ConvNeXt-L. Here, we present the sampling time and memory usage for other models. In Tab. 18, we adopt DDPM as the solver and conduct 1000-step sampling. Since the diffusion model in RPG is shared among all the parameter tokens, we can adopt different inference modes to find a balance between memory usage and inference speed:

- **fully parallel:** All tokens are fed into the diffusion model simultaneously. This approach results in a high memory usage but achieves a high generation speed.
- **sequential:** Tokens are fed into the diffusion model one by one. This approach significantly reduces memory usage, as the model only occupies memory for inferring a single token at a time. This enable us to generate parameters of models listed on a GPU with less than 8GB of memory .
- **partially parallel (default):** In partial parallel mode, we set 256 tokens as a batch for the diffusion model inference. This approach significantly boosts speed with a slight increase in GPU memory usage, reaching an optimal trade-off between memory and speed. We adopt this as the default setting.

Based on the results in Tab. 18, our approach can be flexibly applied to many other GPUs as it can achieve a good trade-off between memory and time.

## B.7. Parameter sensitivity v.s. performance

According to conventional understanding, larger parameter quantities are generally more challenging to learn. However, our experiments reveal that this rule is not absolute and demonstrates instability in learning some small model parameters.

This motivates us to investigate the relationship between parameter sensitivity and generation quality. Specifically, we add Gaussian noise with weights of 0.01, 0.10, and 1.00 to the original parameters to measure model sensitivity, as shown in Tab. 19. We observe that as noise weight increases, performance decreases for all models, with smaller models being more affected than larger ones. This indicates that smaller models are relatively more sensitive. Additionally, we notice that the performance gap between the original and generated models widens as sensitivity of the model increases. This demonstrates a strong correlation between a model’s sensitivity and the difficulty of generating its parameters.

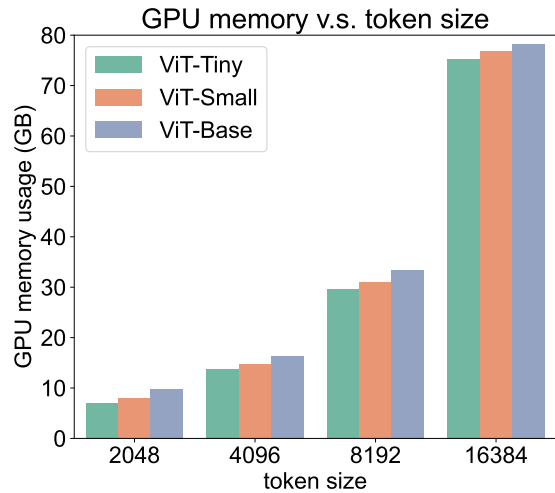
## B.8. Why not auto-regression?

It is worth noting that our approach does not employ an auto-regressive method, *i.e.*, we do not feed the output back as input again. Our method takes position embedding and permutation state as inputs and synthesizes neural network parameters as outputs, forming a standard recurrent neural network. We have attempted to train our model using an auto-regressive approach such as a decoder-only transformer architecture, whose results are shown in Tab 17. Due to the accumulation of errors during the auto-regressive process in inference, the parameters generated at the end of sequence become nearly indistinguishable from noise, leading to poor performance. In contrast, in RPG, noise is only introduced in the diffusion model and does not accumulate in the recurrent process, ensuring stable parameter generation.

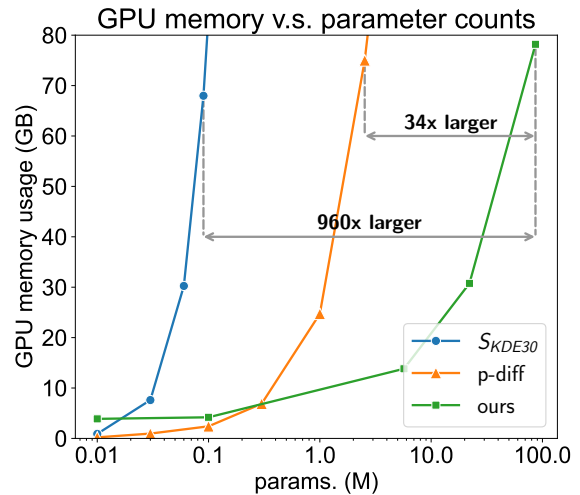
	best	avg.	min.
original	75.2	74.9	74.7
auto-regressive	fail	fail	fail
non-auto-regressive	75.0	74.8	74.6

Table 17. Comparison between auto-regressive and non-auto-regressive methods. The auto-regressive model refers to a transformer decoder-only structure, while the non-auto-regressive model refers to a transformer encoder-only structure with the same scale. To ensure a fair comparison, we also applied a causal mask to the transformer encoder-only structure, ensuring that information can only be passed in one direction.





(a) Visualization of GPU memory v.s. token size. GPU memory usage increases proportionally to the token size. Thus, the token size cannot get larger infinitely; we need to choose a proper token size.



(b) Visualization of GPU memory v.s. parameter counts. Our method can generate much more parameters than existing approaches e.g.  $S_{KDE30}$  [58] using a single NVIDIA H100 80G GPU.

Figure 8. Training memory cost analysis. *Left*: GPU memory v.s. token size. *Right*: GPU memory v.s. parameter counts.

metrics	inference mode	ResNet-18	ResNet-50	ViT-Tiny	ViT-Small	ConvNeXt-A
time (minute)	sequential	18.6	38.0	9.8	33.8	6.8
	partially parallel	1.8	3.3	1.1	2.9	0.9
	fully parallel	1.7	3.3	1.1	2.9	0.9
memory cost (GB)	sequential	6.3	6.4	6.2	6.4	6.2
	partially parallel	10.3	10.5	10.3	10.5	10.3
	fully parallel	30.8	50.5	19.4	45.9	15.2

Table 18. We show the inference time and memory cost under different inference modes. All information in this table is collected from a single NVIDIA H100 80G GPU. We report the time and memory required to generate a single model.

model	params. (M)	sensitivity	accuracy decline			
			ours	noise (0.01)	noise (0.10)	noise (1.00)
ConvNeXt-A	3.7	+++	0.85	62.83	0.60	0.03
ResNet-18	11.7	++	0.39	53.56	0.46	0.00
ViT-Base	86.6	+	0.09	5.39	0.02	0.00

Table 19. The accuracy decline reflects the accuracy gap between the original model and the generated model or the model after adding noise. We add Gaussian noise with weights of 0.01, 0.10, and 1.00 to the parameters to measure model sensitivity. Results demonstrate that smaller models are relatively more sensitive than larger ones. The more plus signs (+), the higher the sensitivity.